The Bioscan
AN INTERNATIONAL QUARTERLY JOURNAL OF LIFE SCIENCES
21(3): 154-164, 2026
www.thebioscan.com

Integrated Network Pharmacology and Molecular Dynamics Simulation to Evaluate the Anti-Osteoporotic Efficacy of Radish (*Raphanus sativus*) Seeds

Sneha Hajare[1], Sanjay Ugare[1*], Sachin Gudasi[2], Santosh Nidagundi[1], Iqra Mujawar[1]

[1]Department of Pharmacology and Toxicology, KLE College of Pharmacy, Belagavi, KLE Academy of Higher Education and Research, Belagavi, Karnataka 590 010, India.
[2]Department of Pharmacognosy, KLE College of Pharmacy, Belagavi, KLE Academy of Higher Education and Research, Belagavi, Karnataka 590 010, India.

Corresponding Author: Dr. Sanjay Ugare , sanjayugare@klepharm.edu , +91-9481004291

DOI: https://doi.org/10.63001/tbs.2026.v21.i03.pp154-164

KEYWORDS
***Raphanus sativus*, Osteoporosis, Dexamethasone, Network Pharmacology, Molecular Docking, Antioxidant.**
Received on:25-06-2026
Revised on:29-06-2026
Accepted on: 04-07-2026
Published on: 20-07-2026

Abstract

Glucocorticoid-induced osteoporosis (GIO), a prevalent secondary bone disorder driven by suppressed bone formation, heightened resorption, and oxidative stress, prompts the exploration of natural alternatives to conventional treatments burdened by side effects; thus, this study investigates the anti-osteoporotic potential and molecular mechanisms of Raphanus sativus seed extract against dexamethasone-induced bone loss via an integrated computational and experimental approach. Bioactive compounds from R. sativus seeds were sourced from literature and databases, with network pharmacology revealing 33 phytocompounds and 219 overlapping targets with GIO; hub proteins such as TNF, STAT3, NFKB1, and PIK3R1 emerged from PPI networks, linked to inflammatory signaling and bone remodeling, while KEGG enrichment underscored PI3K-Akt and osteoclast differentiation pathways. Molecular docking and dynamics (MD) simulations confirmed stable binding of lead compounds-Castasterone to NFKB1 and S-methyl-L-cysteine sulfoxide to PIK3R1-while in vitro assays demonstrated potent antioxidant activity (DPPH IC_{50}: 58.24 µg/mL; NO IC_{50}: 62.22 µg/mL) alongside high total phenolic content (TPC: 76.30 mg GAE/g) and flavonoid content (TFC: 44.7 mg QE/g). These findings elucidate how R. sativus seeds protect against glucocorticoid-induced bone damage by modulating inflammation, countering oxidative stress, and restoring bone homeostasis, laying a mechanistic groundwork for its development as a natural therapeutic for osteoporosis management.

1. INTRODUCTION

The World Health Organization (WHO) defined osteoporosis in 1993 as a systemic skeletal disorder characterized by compromised bone mass and microarchitectural integrity, resulting in augmented bone fragility and heightened fracture susceptibility (1). Furthermore, osteoporosis is characterized by a dysregulation in bone cell function (2). According to WHO criteria, osteoporosis is diagnosed when an individual's bone mineral density (BMD) is 2.5 standard deviations or more below the mean BMD of a healthy young female reference population, corresponding to a T-score of ≤ -2.5(3). A recent study reported a global prevalence of 19.7% for osteoporosis and osteopenia, whereas an economic analysis estimated the worldwide annual cost of osteoporosis to be approximately 56.9 billion USD in 2019(4,5). Osteoporosis, termed 'the silent epidemic of the 21st century', is a prevalent, chronic metabolic bone disorder that often remains asymptomatic until a fracture occurs, leading to significant public health impact (6,7).Osteoporosis is broadly classified into primary and secondary types (8). Primary osteoporosis results from aging or menopause, whereas secondary osteoporosis stems from underlying conditions (e.g., rheumatoid arthritis) or medication use (e.g;glucocorticoids) (9). Long-term glucocorticoid (GC) therapy, commonly used for inflammatory and autoimmune conditions, often leads to osteoporosis, with 30-50% of chronic users experiencing fractures (10).

GC-induced osteoporosis pathogenesis primarily involves effects on osteoblasts, osteocytes, and osteoclasts (11). Glucocorticoids (GCs) impair bone formation and enhance resorption via direct and indirect mechanisms, including reduced calcium absorption, elevated PTH, downregulation of osteogenic genes (e.g., osteocalcin), increased osteoblast apoptosis, and stimulated osteoclast activity. (12,13).

Protein kinase B (Akt) plays a vital role in cell survival mechanisms, particularly through the phosphatidylinositol 3-kinase (PI3K)/Akt signaling pathway. Activation of this pathway has been shown to promote osteoblast proliferation, differentiation, and bone formation, while also inhibiting apoptosis, thereby helping to counteract osteoporosis (14). Downregulating the PI3K/Akt pathway, in turn, has been linked to GC-induced bone damage in both in vitro and in vivo studies (15). Oxidative stress plays a substantial role in the development of osteoporosis and various other diseases (16). Oxidative stress arises from an imbalance between reactive oxygen species (ROS) production and the body's antioxidant defenses, leading to tissue damage. DEX has been shown to increase ROS levels, inducing osteoblast apoptosis, promoting osteoclast formation, and resulting in bone loss (17).

Current osteoporosis treatments include estrogen, SERMs, bisphosphonates, calcitonin, rhPTH, and denosumab, which target bone resorption and formation pathways. (18,19). Despite their efficacy, many currently available osteoporosis medications have significant drawbacks, including contraindications and severe side effects. For instance, bisphosphonates, a commonly prescribed first-line treatment for osteoporosis, are not suitable for patients with kidney problems or gastrointestinal issues and have been linked to several safety concerns, both short-term and long-term. Two rare but particularly serious adverse

effects associated with bisphosphonate use are osteonecrosis of the jaw and atypical femoral fractures. Furthermore, denosumab has been associated with severe hypocalcaemia in some patients, highlighting the need for careful consideration and monitoring when using these medications. Additionally, the development of alternative therapeutic strategies is necessary to provide safer and more effective treatment options for patients with osteoporosis (20-23).

Globally, herbal remedies are acknowledged for their medicinal properties, providing advantages over synthetic pharmaceuticals, including reduced toxicity and side effects, and continuing to play a vital role in traditional and modern healthcare.

The Brassicaceae family comprises *Raphanus sativus*, a commonly cultivated vegetable. (24). *Raphanus sativus* components (seeds, roots, leaves) are used in traditional medicine. Radish seeds (Raphani Semen) treat digestive, respiratory, and inflammatory disorders in Chinese, Korean, and Indian medicine. (25). Radish seeds contain bioactive compounds (glucosinolates, alkaloids, terpenoids, polyphenols) with anti-tumor, anti-inflammatory, antioxidant, anti-diabetic, and anti-obesity properties. Glucoraphenin, a key glucosinolate, regulates lipid metabolism and improves metabolic disorders (26). *Raphanus sativus* extracts exhibit diverse bioactivities, including antioxidant, antimicrobial, antihypertensive, antitussive, antiasthmatic, neuroprotective, and anti-osteoporotic effects. (25).

The available evidence suggests R. sativus possesses anti-osteoporotic potential. This study employs a combined in-silico and in-vivo approach to evaluate its efficacy, elucidating molecular mechanisms and assessing therapeutic effects in a dexamethasone-induced osteoporosis model, thereby validating R. sativus as a natural alternative for osteoporosis management.

2. MATERIALS & METHODS

In-silico studies:

Identification of Metabolites and their Potential Target Proteins:

Phytoconstituents previously reported in the seeds of *Raphanus sativus* were collected from diverse sources, including scientific literature, traditional medicinal texts, and databases such as IMPPAT (https://cb.imsc.res.in/imppat/) and Dr. Duke's Phytochemical Database(https://phytochem.nal.usda.gov/) (27). The corresponding PubChem C IDs were retrieved from the PubChem database (https://pubchem.ncbi.nlm.nih.gov), and their SMILES notations were curated accordingly. The SuperPred tool(https://pubchem.ncbi.nlm.nih.gov) was employed to predict the probable protein targets of the selected phytoconstituents based on their SMILES. Subsequently, the gene names of the identified target proteins were extracted from the UniProt databases(UniProtKB, http://www.uniprot.org/)), with the organism filter set to "Homosapiens" (28).

Prediction of disease related targets-gene card:

Using the keyword 'Dexamethasone-induced osteoporosis,' a comprehensive search was conducted on the Gene Cards database along with relevant literature mining to identify key genes and protein targets associated with the pathogenesis of glucocorticoid-induced bone loss. The identified gene targets provided insights into the molecular mechanisms underlying osteoporosis (29).

Overlap Analysis of *Raphanus sativus* Phytoconstituent's and Osteoporosis-linked Genes:

The common targets shared between the phytoconstituents and osteoporosis-related genes were identified using the Venny 2.0 tool.

Protein-protein interaction:

Protein-protein interaction (PPI) networks were generated and depicted using the STRING database through inputting overlapping genes. The resulting interaction data were then transferred to Cytoscape for centrality analysis, in which nodes denoted target proteins and edges represented their interactions. STRING evaluated mutual interaction scores for each protein, exhibiting higher values indicating greater associations. Unconnected (isolated) nodes were filtered out, and the network was constructed using a minimum confidence score cutoff of 0.04. Further, cluster analysis was conducted using the MCODE clustering module plugin in Cytoscape 3.10.2 (30,31).

Network generation and analysis:

The network linking the phytochemicals of *Raphanus sativus* with their corresponding targets was constructed using Cytoscape 3.10.2. Interactions between the bioactive compounds and target genes were subsequently visualized and analyzed employing the "Network Analyzer" tool, with edge counts ranked from highest to lowest to evaluate modulatory potential. Network analysis was performed based on parameters such as node degree distribution and betweenness centrality, along with additional metrics including eccentricity, neighborhood connectivity, in-degree distribution, and out-degree distribution. Within this network, nodes denoted compounds, targets, and pathways, whereas edges represented the interactions among these entities, thereby illustrating the association between bioactive constituents and disease-related targets. The degree value of interactions was used to assess the importance of nodes in each network (32).

Gene Ontology and KEGG Pathway Enrichment Analyses for Osteoporosis-Associated Targets via the Clue GO and Clue Pedia Plugins.

Gene Ontology (GO) and KEGG pathway enrichment analyses were performed using the Clue(https://apps.cytoscape.org/apps/cluego) GO and CluePedia(https://apps.cytoscape.org/apps/cluepedia) plugins within the Cytoscape platform. ClueGO was utilized to visualize and interpret functional annotations associated with gene sets and biological pathways. The tool applies statistical methods, such as the hypergeometric test, to assess enrichment significance, thereby identifying key biological processes and pathways relevant to the dataset. CluePedia was employed alongside ClueGO to facilitate a more comprehensive exploration of pathway interactions. This complementary plugin enabled the identification of potential novel biomarkers and the elucidation of relationships between genes and pathways, providing an integrated understanding of the biological relevance of the data (33,34).

Molecular docking:

Molecular docking analyses were performed to assess the binding affinities of selected bioactive compounds against pivotal target proteins. Simulations were executed using Auto Dock/Vina or equivalent molecular modeling software. Binding interactions were evaluated based on docking scores, particularly focusing on binding free energy (kcal/mol), hydrogen bond formation, and hydrophobic contacts, thereby facilitating the prediction of the compounds' potential to modulate target protein function (35,36).

Molecular Dynamics:

Molecular dynamics (MD) simulations of phosphoinositide 3-kinase delta (PI3Kδ) in complex with compound 15 were conducted using the Desmond module of the Schrödinger Suite. The protein-ligand complex obtained from molecular docking was prepared utilizing the Protein Preparation Wizard, wherein missing hydrogen atoms were added, bond orders were assigned, disulfide linkages were generated, and protonation states were optimized at physiological pH. The system was subsequently minimized under the OPLS force field to eliminate steric clashes. The prepared complex was then placed within an orthorhombic simulation box and solvated using the TIP3P water model, maintaining a buffer distance of 10 Å. Appropriate counterions were introduced to neutralize the system, and 0.15 M NaCl was added to simulate physiological ionic conditions. Energy minimization followed by a stepwise equilibration

protocol under NVT and NPT ensembles was performed prior to the production phase. The production MD simulation was executed under periodic boundary conditions at 300 K and 1 atm pressure, employing the Nosé-Hoover thermostat and Martyna-Tobias-Klein barostat. Trajectory analyses were subsequently performed to evaluate root mean square deviation (RMSD) and overall system stability(37).

Preparation of Extract:

The seeds of *Raphanus sativus* were obtained from the local market of Belagavi, Karnataka, India, during June. The plant material was authenticated at the Central Research Facility, Shri B. M. K. Ayurveda Mahavidyalaya, Belagavi, & a voucher specimen was deposited for future reference under the authentication number BMK/CRF/479/2025-26. The collected seeds were cleaned thoroughly to remove any impurities and were shade-dried at room temperature. After complete drying, the seeds were coarsely powdered using a mechanical grinder. The powdered material was then extracted by the maceration method using a hydroalcoholic solvent system (ethanol: water, 70:30 v/v) for a duration of 72 h at room temperature with periodic stirring to ensure proper extraction. The mixture was filtered, and the solvent was removed under reduced pressure using a rotary evaporator. The resulting dried extract was stored in an airtight container at 4 °C until it was used for further experimental studies(38).

In vitro antioxidant activity:

DPPH radical scavenging assay:

The free radical scavenging activity of the *Raphanus sativus* extract was evaluated using the DPPH (1,1-diphenyl-2-picrylhydrazyl) assay, following the method described by Baliyan et al. (2022) with slight modifications. The extract was dissolved in methanol and assessed using a 0.1 mM DPPH solution. Ascorbic acid was used as a standard antioxidant control. Serial concentrations of both the extract and the standard (20, 40, 60, 80, and 100 µg/mL) were prepared. An aliquot of each concentration (1 mL) was mixed with 3 mL of the DPPH solution in separate volumetric flasks. A similar procedure was followed for ascorbic acid. The reaction mixtures were incubated in the dark for 30 min to facilitate the reaction. Subsequently, absorbance was measured at 517 nm using UV-visible spectrophotometer (39). The percentage of radical scavenging activity was then calculated using the formula:

%"Antioxidant Activity"=(Abs control-Abs sample)/(Abs control)×100

Nitric oxide (NO) scavenging activity assay:

The nitric oxide radical scavenging activity of the *Raphanus sativus* extract was evaluated by incubating varying concentrations (20-100 µg/mL) of the extract with 10 mM sodium nitroprusside for 150 min. Following incubation, Griess reagent was added, and the absorbance of the resulting chromophore was measured at 590 nm (40).The percentage inhibition and IC_{50} values for varying concentrations were evaluated.

The formula for calculating percentage inhibition of NO radicals is:

% Inhibition =(Control Abs-Sample Abs)/(Control Abs)×100

Total Flavonoid content:

The total flavonoid content of the *Raphanus sativus* extract was quantified using a modified colorimetric method adapted from Sulastri et al. (2018)(41).The total flavonoid content of the *Raphanus sativus* extract was quantified using a modified colorimetric method adapted from Sulastri et al. (2018). A quercetin stock preparation (10 mg in 100 mL of 90% aqueous methanol, equivalent to 100 µg/mL) was serially diluted to obtain concentrations of 10, 20, 40, 60, 80, and 100 µg/mL. For each standard, 0.5 mL of the respective dilution was combined with 1.5 mL of 90% aqueous methanol, 0.1 mL of 10% aluminum chloride, 0.1 mL of 1 M potassium acetate, and 2.8 mL of distilled water. The reaction mixtures were incubated at room temperature for 30 minutes, after which the absorbance was measured at 415 nm using a UV–Visible spectrophotometer. A blank was prepared under identical conditions by substituting aluminum chloride with an equal volume of distilled water. The extract preparation was carried out by dissolving 1 g of the sample in 25 mL of 90% aqueous methanol, followed by treatment with aluminum chloride under the same experimental conditions. All determinations were performed in duplicate. The flavonoid content was calculated from the calibration curve constructed using quercetin, plotting absorbance against concentration.

Total phenolic content:

The total phenolic content was determined using the Folin-Ciocalteu reagent according to a method adapted from Sulastri et al. (2018) (41). A calibration curve was generated using gallic acid as the reference standard at concentrations ranging from 5 to 125 µg/mL. The sample preparation involved dissolving 10 mg of the extract in 10 mL of methanol. For both standard and sample preparations, 0.5 mL aliquots were mixed with 2.5 mL of 50% Folin-Ciocalteu reagent and 2.5 mL of distilled water. Following an incubation period of 5 minutes, 2 mL of 7.5% (w/v) aqueous sodium carbonate solution was added. The reaction mixture was thoroughly mixed and incubated in the dark at room temperature for 15 minutes. Subsequently, the absorbance was recorded at 765 nm using a UV–Visible spectrophotometer. The total phenolic content was expressed as micrograms of gallic acid equivalents per milli liter of extract, based on the calibration curve.

3. RESULTS:

3.1 Network Pharmacology

3.1.1 Identification of Phytocompounds and Disease-Related Targets:

A total of 33 phytocompounds were identified from the seeds of *Raphanus sativus*. Target prediction using the SuperPred database revealed 219 potential protein targets associated with these phytocompounds. Additionally, 1904 protein targets modulated by dexamethasone and potentially associated with mechanisms of disease development of osteoporosis were sourced from public accessible databases, including GeneCards. These targets are associated with dexamethasone-induced alterations in bone metabolism and related complications.

3.1.2 Identification of Common Targets for Pathway Analysis:

The protein targets obtained from the seeds of *Raphanus sativus* and dexamethasone-induced osteoporosis were compared using the Venny 2.0 tool. A total of 219 overlapping protein target were identified and subsequently used for pathway enrichment analysis (Figure 1).

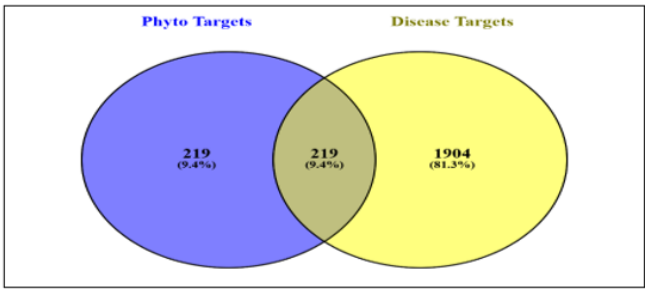

*(Figure 1): Common targets between Phyto targets and Diseases targets.

Protein-protein interaction network of *Raphanus sativus* – Osteoporosis disease linked genes:

The protein-protein interaction (PPI) network of *Raphanus sativus* in osteoporosis reveals a multi-target regulatory mechanism acting on inflammatory, hypoxic, and osteoclastogenic pathways (Figure 2). Hub proteins such as TNF (151), STAT3 (124), and NFKB1 (105) indicate strong modulation of inflammatory signaling that drives osteoclast differentiation. Activation of EGFR (112) and MTOR (83) suggests involvement in osteoblast proliferation and bone remodeling. HIF1A (97) reflects hypoxia-mediated bone resorption, while MMP9 contributes to extracellular matrix degradation. PTGS2 (87) and TLR4 (86) further amplify inflammatory cascades. The presence of ESR1 (99) highlights estrogen-dependent bone protection.

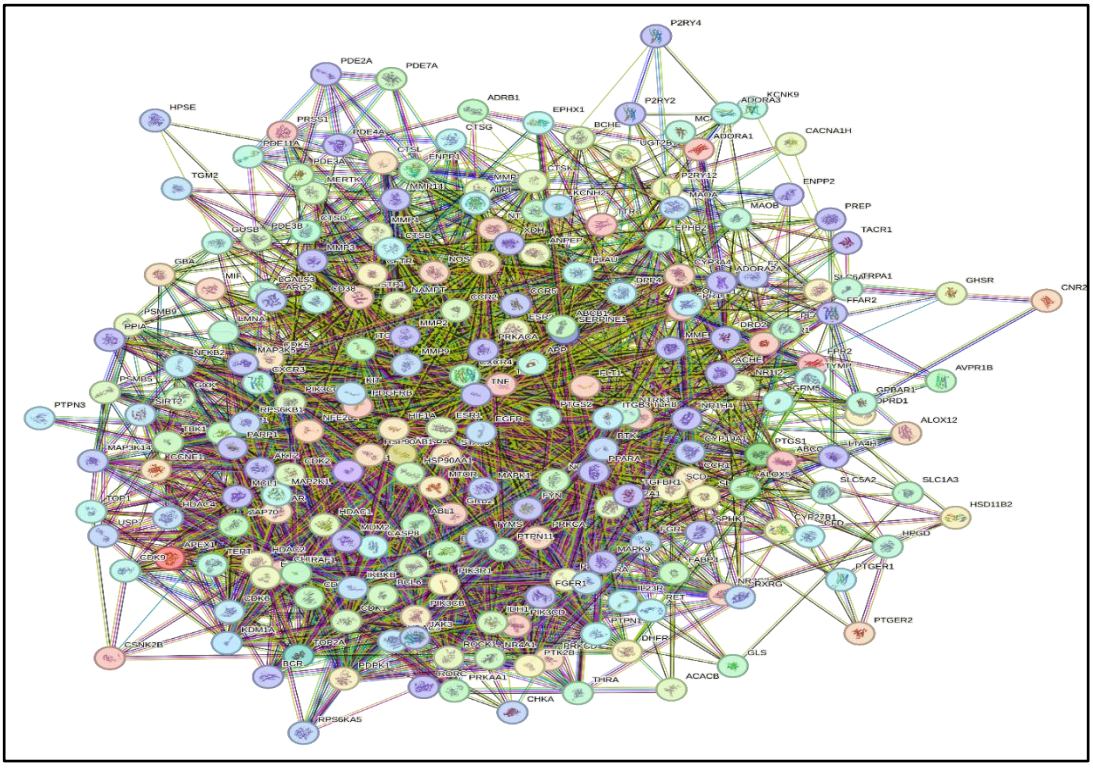

Figure 2): The protein-protein interaction (PPI) network of *Raphanus sativus* in osteoporosis.

3.2 GO and KEGG pathway enrichment analyses for PPI network:

3.2.1 Gene Ontology:

The Gene Ontology (GO) analysis demonstrates that the treatment of osteoporosis involves a coordinated interplay of biological processes, cellular components, and molecular functions that in combination regulate bone remodeling, inflammation, oxidative stress, and cellular signaling (Figure 3). Key biological processes including response to organic substances, chemicals, and stimuli (GO:0010033; GO:0042221; GO:0050896) highlight the influence of hormones, cytokines, and metabolic signals on osteoblast and osteoclast activity. Genes such as MAPK1, PI3KCA, AKT2, STAT3, EGFR, ESR1, and TNF modulate osteogenesis, inhibit osteoclast differentiation, and maintain bone matrix homeostasis. Processes linked to oxidative stress, such as response to oxygen-containing compounds (GO:1901700) and cellular response to chemical stimulus (GO:0070887), involve genes including NFE2L2, HIF1A, and SIRT2, which protect bone cells from oxidative damage. Immune and endocrine regulatory processes mediated by TLR4, CXCR4, NFKB1, ESR1, PPARA, and TGFBR1 further support inflammation control and balanced bone turnover. At the cellular component level, enriched locations such as the plasma membrane, cell periphery, cytoplasm, vesicles, endomembrane system, and intracellular organelle lumen indicate that therapeutic mechanisms span membrane signaling, intracellular cascade activation, vesicular trafficking, and nuclear regulation. Membrane-bound receptors and integrins (EGFR, CCR1/2/5, CXCR4, ITGB1/3) facilitate cell communication, while cytoplasmic kinases (MAPK1, AKT2, MTOR, NF-κB) drive osteogenic differentiation and survival. Vesicle-associated proteins including MMP14, PLAT, CTSB/L regulate matrix remodeling, whereas nuclear components such as ESR1, RXRA, HDACs, and PARP1 govern

transcriptional control and hormonal signaling. At the molecular-function level, enriched catalytic activity, kinase activity, protein binding, enzyme binding, ion binding, and small-molecule binding underscore the roles of enzymes, kinases, and receptors in bone metabolism. Critical enzymes like MMPs, CTSK, ALPL, PTGS2, and PARP1 regulate matrix turnover and mineralization, while kinases (PI3K, EGFR, RAF1, JAK3, TGFBR1) activate pathways essential for bone formation and osteoclast inhibition. These integrated GO functions reveal that osteoporosis treatment restores skeletal homeostasis by reducing inflammation and oxidative stress, enhancing osteoblast activity, and suppressing excessive bone resorption.

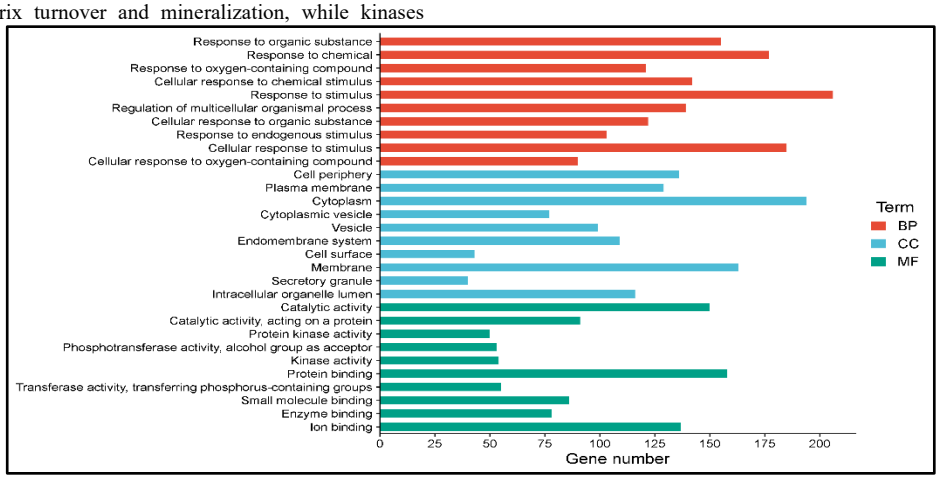

Figure 3): Gene Ontology (GO) enrichment analysis.

3.2.2 KEGG Pathway:

The KEGG pathway analysis reveals that the genes implicated in osteoporosis are strongly enriched in signaling networks that regulate bone remodeling, osteoclastogenesis, oxidative stress, inflammation, and hormonal control of skeletal homeostasis (Figure 4). The phosphoinositide 3-kinase (PI3K)-Akt signaling pathway, one of the most strongly enriched pathways, includes key genes such as PIK3CA, PIK3R1, AKT2, MTOR, PDPK1, and GRB2, which collectively promote osteoblast survival, suppress apoptosis, and regulate bone formation; dysregulation of this pathway contributes to reduced bone mass and enhanced osteoclast activity in osteoporosis. The Osteoclast differentiation pathway, enriched with genes such as NFKB1, MAPK1, CTSK, STAT1, CHUK, IKBKB, BTK, and TNF, directly drives the activation and maturation of osteoclasts, thereby increasing bone resorption, a hallmark of osteoporosis. The MAPK signaling pathway, involving MAPK1, MAPK9, RAF1, EGFR, and PDGFRB, further influences osteoblast proliferation, osteoclast development, and inflammatory responses, linking cellular stress to bone degradation. Likewise, the TNF signaling pathway, with genes like TNF, PTGS2, CASP8, and MAP3K14, amplifies inflammation-induced bone resorption by activating NF-κB and MAPK cascades. Hormonal pathways, particularly the Estrogen- and Thyroid hormone–mediated signaling pathways, enriched with genes such as ESR1, ESR2, THRA, and RXRA, highlight the crucial role of endocrine regulation in bone turnover, reflecting how estrogen deficiency accelerates osteoclast activity in postmenopausal osteoporosis. Additionally, HIF-1, FoxO, and AGE-RAGE pathways contribute to oxidative stress, impaired osteoblast function, and chronic inflammation. Overall, the combined enrichment of these pathways indicates that osteoporosis arises from the convergence of inflammatory, hormonal, oxidative, and differentiation-related molecular processes that shift bone remodeling toward excessive resorption and diminished formation.

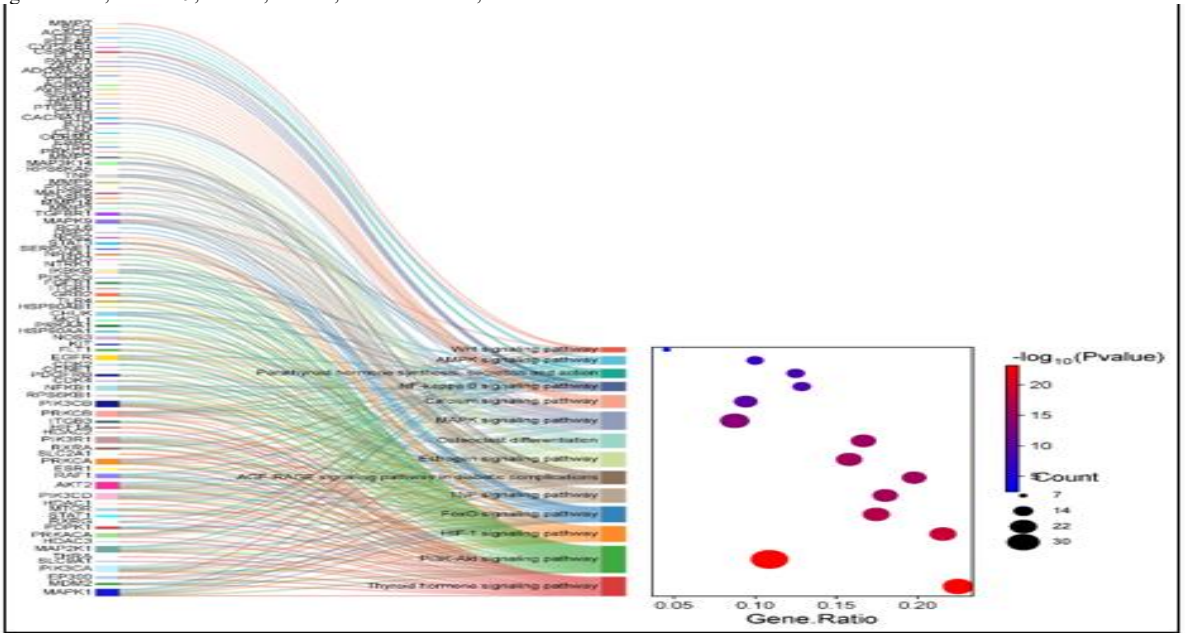

Figure 4): KEGG pathway analysis.

3.3 Network Pharmacology Analysis of *Raphanus sativus*

Network was constructed by importing Compound - targets-pathway file to the cytoscape 3.10.1 to analyse the relation between the compounds, targets and pathways (Figure 5). The resulting network contained 137 nodes and 889 edges, reflecting a densely interconnected regulatory architecture. Topological analysis was performed using the Network Analyzer module, with degree centrality applied to identify hub proteins. NFKB1 (degree = 31), PIK3R1 (degree = 28), and CTSD (degree = 26) emerged as the principal hubs, demonstrating extensive connectivity across multiple compounds and signaling pathways, thereby highlighting their central roles in mediating the collective pharmacological effects. Additional high-ranking nodes included PIK3CD, PRKCA, CHUK, SCD, TLR4, PIK3CB, PRKCB, PIK3CA, SLC9A1, PRKCD, CCNE1 and NR4A1 indicating strong convergence on proliferative and survival signaling networks. The PI3K–Akt signaling pathway was identified as the most prominently modulated pathway in the analysis, incorporating 38 associated targets. Thyroid hormone signaling pathway ranked as the second most significantly modulated pathway, encompassing 27 targets, further supporting the relevance of these phytochemicals in modulating key molecular events implicated in liver cancer progression. Among all the compounds 1-Tetradecene and 1-Hexadecene is highly modulated compound with 35 targets (Figure 5).

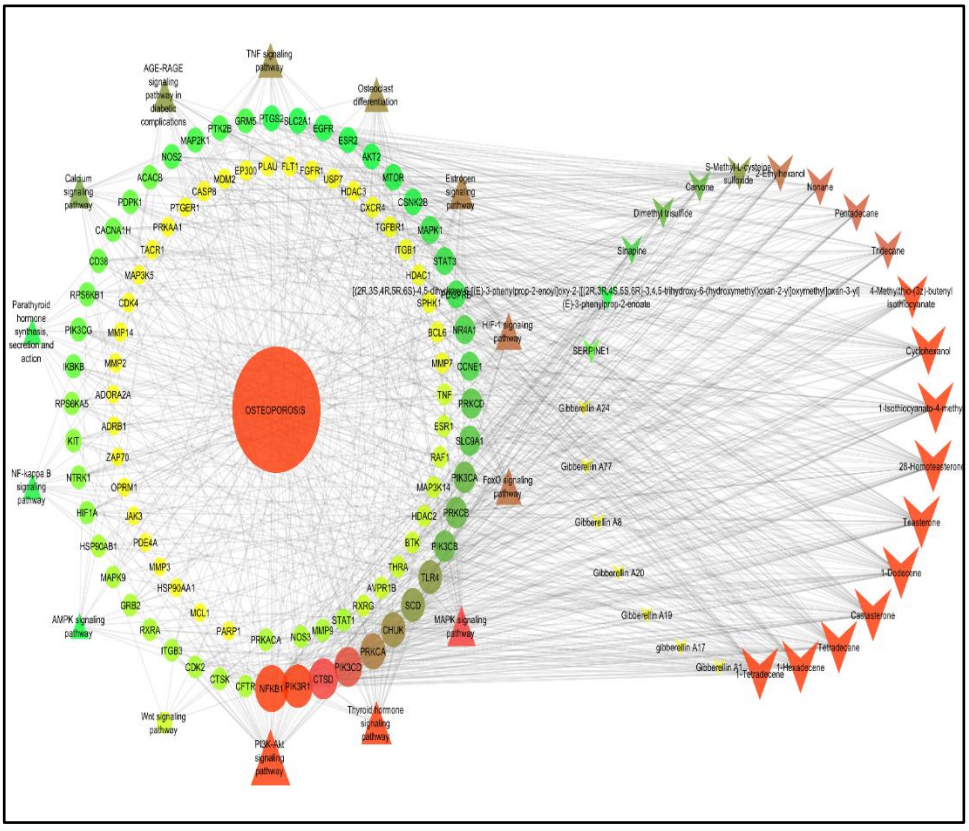

(Figure 5): Network Pharmacology of *Raphanus sativus* compounds against osteoporosis

3.4 Molecular docking:

Molecular docking analysis was carried out to evaluate the binding affinity and interactions of phytoconstituents from *Raphanus sativus* with the target proteins NFKB1 (PDB ID: 1NFI) and PIK3R1 (PDB ID: 6OCO). Docking simulations were carried out using the Schrödinger Suite (version 2020-1), and ligand-protein interactions were analyzed and visualized through the Maestro platform. The analysis aimed to investigate the binding affinity and molecular interaction patterns of selected compounds within the active sites of these lipid-associated regulatory proteins (Table1) (Figure: 6 &7).

For the NFKB1 structure (PDB ID: 1NFI), the phytoconstituent Castasterone (C20) demonstrated a docking score of - 4.626 kcal/mol and a Glide energy of-32.550 kcal/mol. The compound established several hydrogen-bond interactions with critical amino acid residues, including ARG30, ASN190, GLN230, GLN247, and ARG158 within the binding pocket (Figure :6). In comparative analysis, the reference drug Alendronate (S1) exhibited a slightly stronger docking score of -4.707 kcal/mol and a Glide energy of -34.625 kcal/mol, forming hydrogen-bond interactions with ASN190 and THR191. These results suggest that castasterone demonstrates a comparable binding orientation and interaction pattern within the active site of NFKB1, indicating its potential modulatory activity against the target protein(Table1)(Figure :8 &9).

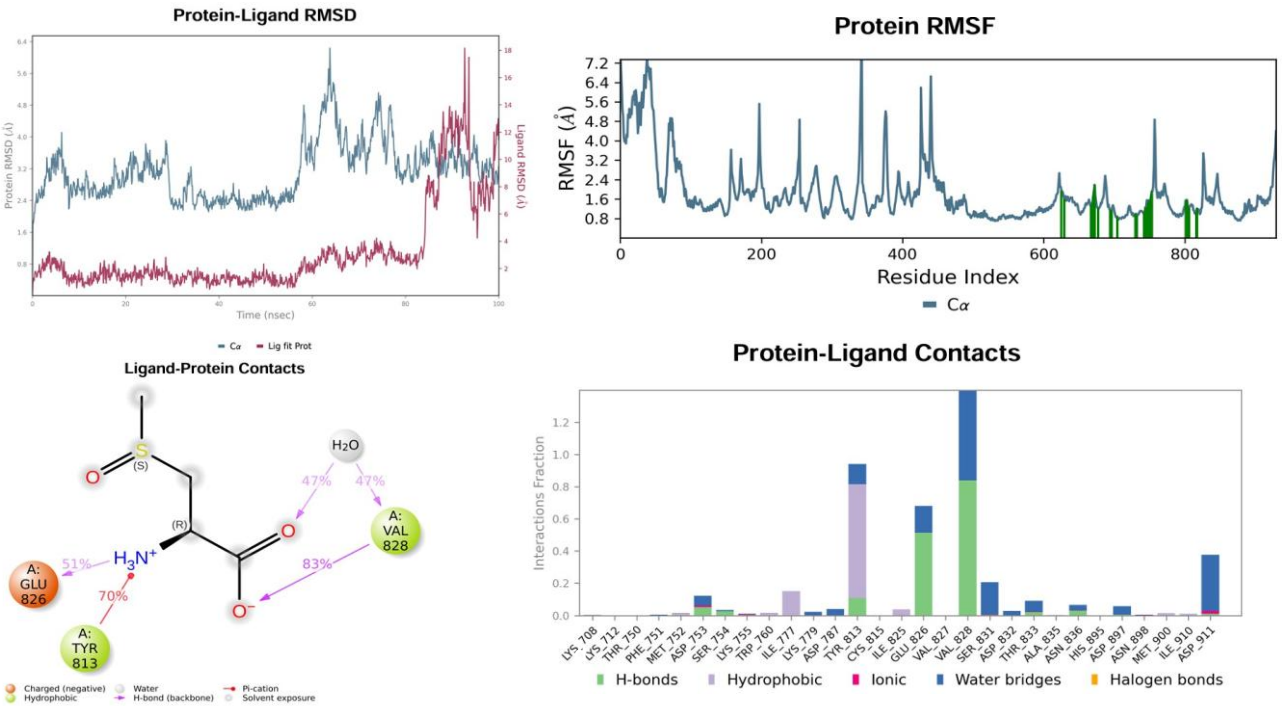

(Figure 10): Molecular dynamics simulation a) Protein ligand RMSD, b) Protein RMSF, c) Ligand-Protein contacts, d) Protein-Ligand Contacts.

***3.5 In Vitro* Antioxidant Assays:**

3.5.1 DPPH ASSAY:

The IC50 of ascorbic acid was calculated and was identified as 34.25 µg/ml and for *Raphanus sativus* seed extract the IC50 was 58.24 µg/ ml. The extract showed the significant scavenging activity compared to Ascorbic acid against DPPH with increasing the %inhibition with the increasing concentration **(Figure 11).**

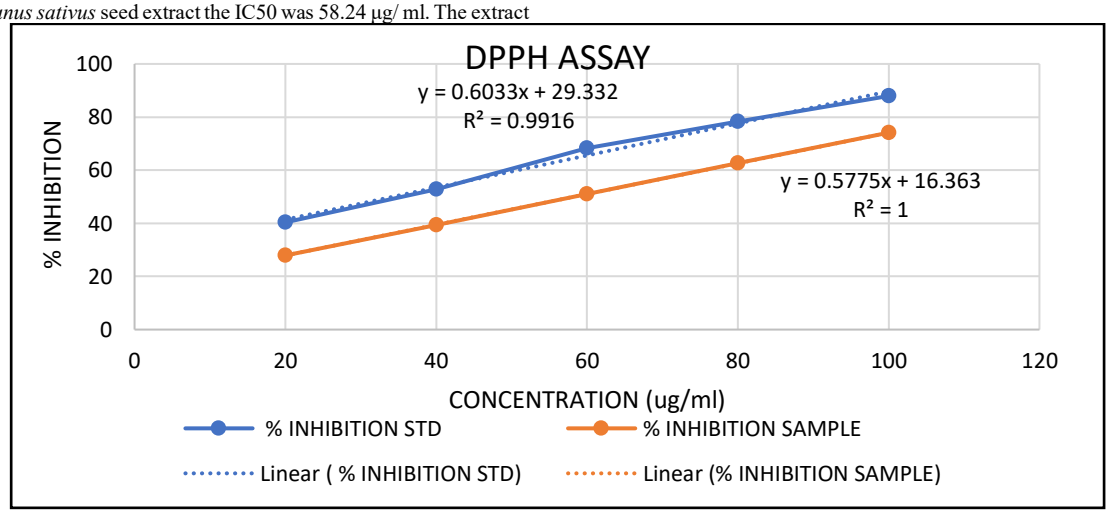

(Figure 11): DPPH ASSAY

3.6 Nitric oxide assay:

The IC_{50} value for ascorbic acid was calculated as 37.14 µg/mL (Y = 0.6033x + 29.332), indicating potent antioxidant activity. In contrast, GSAE demonstrated an IC_{50} value of 62.22 µg/mL (Y = 0.6969x + 3.4375), signifying its appreciable nitric oxide scavenging potential **(Figure:12).**

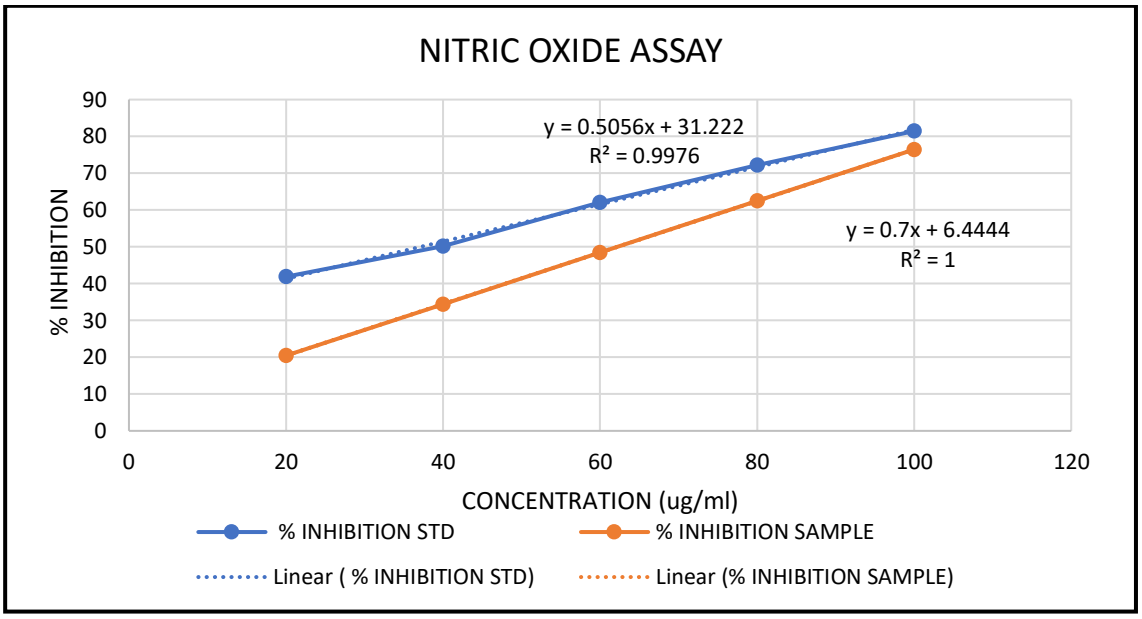

(Figure 12): Nitric oxide assay

3.7 Total Flavonoid Content (TFC) and Total Phenolic Content (TPC):

The total flavonoid content was estimated using the aluminium chloride colorimetric assay. Quantification was carried out based on the regression equation obtained from the quercetin standard calibration curve ($y = 0.001x + 0.02$; $R^2 = 1$). The results were expressed as milligrams of quercetin equivalents per gram of extract (mg QE/g extract). The *Raphanus sativus* extract exhibited a total flavonoid content of 44.7 mg QE/g extract (**Figure 13)**

And total phenol content of *Raphanus sativus* extract was evaluated by gallic acid method, from the regression equation standard plot ($y = 0.013x + 0.02$ $R^2 = 1$) and is expressed in milligram Gallic acid equivalents per gram extract. The total phenol content was observed to be 76.30 mg GAE/g extract **(Figure 14)**

.

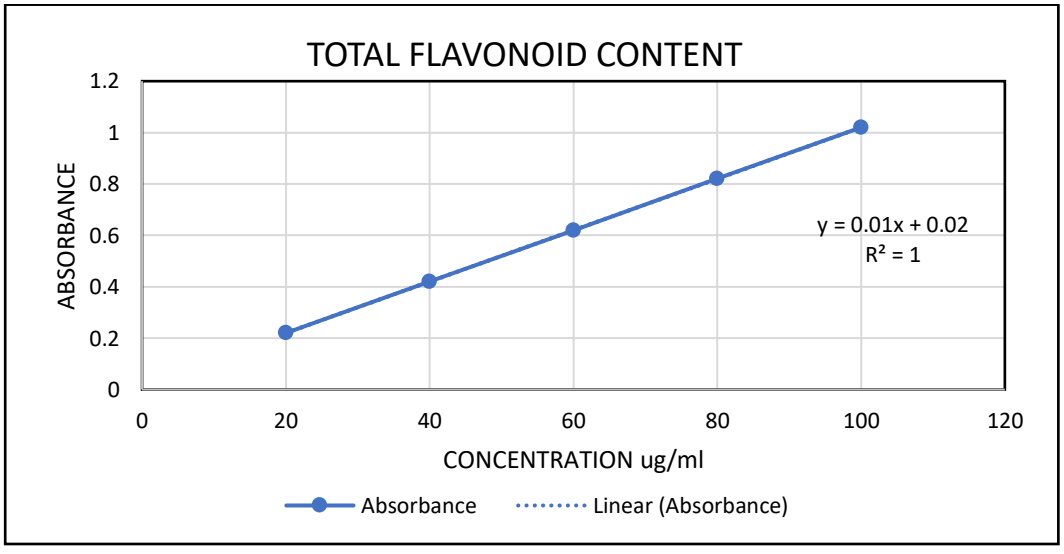

(Figure 13): Total Flavonoid Content

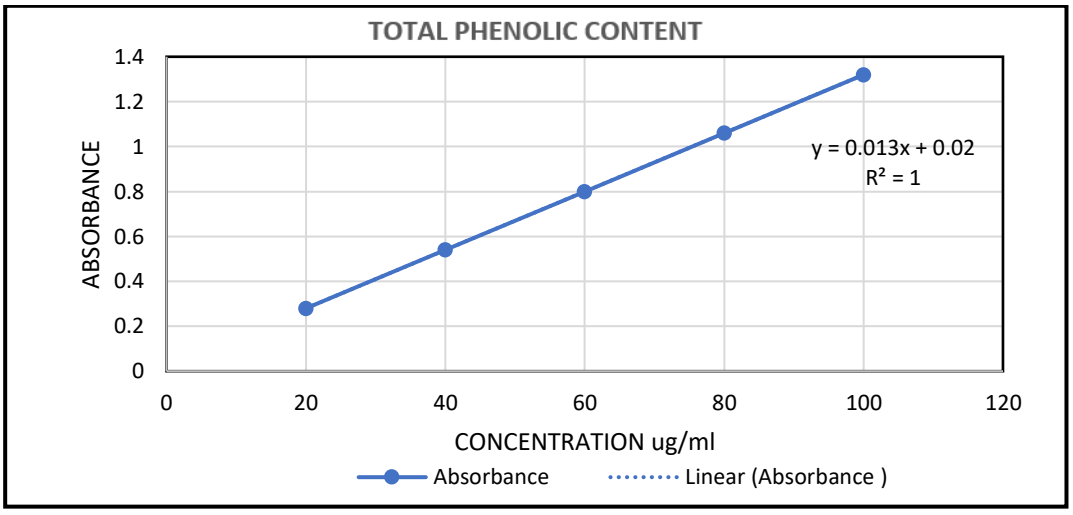

(Figure 14): Total Phenolic Content

4. DISCUSSION

The present investigation elucidates the multi-target anti-osteoporotic potential of *Raphanus sativus* in dexamethasone-induced osteoporosis through an integrated network pharmacology, molecular docking, molecular dynamics, and in vitro antioxidant approach. Glucocorticoid-induced osteoporosis (GIO) is characterized by suppressed osteoblastogenesis, enhanced osteoclast differentiation, oxidative stress, and dysregulation of PI3K/Akt and NF-κB signaling pathways(42,43). The identification of 219 overlapping targets between phytoconstituents and disease-associated genes highlights the pleiotropic regulatory capacity of R. sativus bioactives.

Protein-protein interaction analysis revealed hub nodes including TNF, STAT3, NFKB1, EGFR, MTOR, HIF1A, and ESR1. These hubs are critically implicated in osteoclastogenesis, inflammatory amplification, hypoxia-mediated bone loss, and estrogen-dependent bone preservation. TNF and NF-κB signaling are central drivers of RANKL-mediated osteoclast differentiation, whereas STAT3 integrates inflammatory and survival cues in bone microenvironments. The enrichment of PI3K-Akt and MAPK pathways further supports modulation of osteoblast proliferation and apoptosis resistance, counteracting glucocorticoid-induced suppression of Wnt/β-catenin signalling(44,45).KEGG enrichment confirmed significant association with osteoclast differentiation, TNF signaling, PI3K-Akt signaling, estrogen signaling, and HIF-1 pathways. This convergence indicates that R. sativus may restore skeletal homeostasis by simultaneously suppressing inflammatory osteoclast activation and promoting osteoblast survival. The identification of ESR1 within the core network is particularly relevant in the context of postmenopausal and glucocorticoid-induced bone loss, suggesting phytoestrogen-like modulatory effects(46,47).

Molecular docking provided mechanistic validation of these network predictions. Castasterone demonstrated favorable binding interactions with NFKB1, comparable to alendronate, indicating potential inhibition of NF-κB-mediated transcriptional activation. Similarly, S-methyl-L-cysteine sulfoxide exhibited strong affinity toward PIK3R1, supporting modulation of the PI3K regulatory subunit. Molecular dynamics simulation of PI3Kδ-compound 15 complex further confirmed structural stability, with consistent RMSD profiles and minimal ligand conformational deviation, suggesting sustained binding within the ATP-binding pocket. Such stability implies potential downstream activation of survival signaling in osteoblasts while attenuating glucocorticoid-triggered apoptosis(48,49). Oxidative stress plays a pivotal role in GIO by promoting osteocyte apoptosis and enhancing osteoclast activity. The appreciable DPPH and nitric oxide scavenging activities of the extract, along with substantial total phenolic (76.30 mg GAE/g) and flavonoid (44.7 mg QE/g) contents, indicate robust antioxidant capacity. Polyphenols and glucosinolate derivatives may mitigate ROS-mediated activation of NF-κB and HIF-1α pathways, thereby preserving bone microarchitecture(50). These findings support a systems-level mechanism wherein R. sativus phytoconstituents exert anti-osteoporotic effects through coordinated regulation of inflammatory cytokines, oxidative stress mediators, osteoclast differentiation signals, and pro-survival kinase cascades. The multi-component, multi-target pharmacological profile aligns with contemporary network pharmacology paradigms and suggests therapeutic potential as an adjunct or alternative strategy in glucocorticoid-induced bone loss. Further *in vivo* histomorphometric and biomechanical analyses will be essential to substantiate translational applicability.

5. CONCLUSION

The present study demonstrates that *Raphanus sativus* exhibits significant anti-osteoporotic potential against dexamethasone-induced bone loss through a multi-target pharmacological mechanism. Network pharmacology analysis identified critical hub proteins, including TNF, NFKB1, STAT3, PIK3R1, and ESR1, implicating modulation of inflammatory, osteoclastogenic, and survival signaling pathways. KEGG enrichment further highlighted the involvement of PI3K–Akt, TNF, osteoclast differentiation, and estrogen signaling pathways, indicating restoration of bone remodeling balance. Docking and molecular dynamics simulations revealed stable interactions of key phytoconstituents with NFKB1 and PIK3R1, supporting downregulation of NF-Kb-mediated osteoclast activation as well as enhancement of pro-survival kinase signaling. Additionally, substantial phenolic and flavonoid content correlated with strong antioxidant activity, suggesting attenuation of oxidative stress–induced bone damage. These findings provide mechanistic evidence that R. sativus exerts protective effects through integrated regulation of inflammation, oxidative stress, and osteoblast–osteoclast homeostasis, supporting its potential as a complementary therapeutic strategy for glucocorticoid-induced osteoporosis.

6. ACKNOWLEDGEMENT

The authors are very thankful to Principal Dr. S. S. Jalalpure for his support and guidance. The authors are also thankful to the Department of Pharmacology for their assistance.

CONFLICT OF INTEREST

The authors declare no conflict of interest.

AUTHOR CONTRIBUTION

S.G.: Data curation; formal analysis, investigation; methodology; validation; writing original draft. **Dr. S. U.:** Conceptualization; visualization; project administration; resources; supervision; writing review & editing. **S.G.:** Software, methodology; validation; editing. **I.M.:** Methodology, validation;

editing. **S. N.:** Software; methodology, validation; editing

DATA AVAILABILITY STATEMENT

The data that support the findings of this study are available from the corresponding author upon reasonable request

7. REFERENCES

- Genant HK, Cooper C, Poor G, Reid I, Ehrlich G, Kanis J, Nordin BC, Barrett-Connor E, Black D, Bonjour JP, Dawson-Hughes B. Osteoporos. Int. 1999;10(4):259.
- Letarouilly JG, Broux O, Clabaut A. Genomics. 2019;111(4):793-8.
- Akkawi I, Zmerly H. Joints. 2018;6(02):122-7.
- Xiao PL, Cui AY, Hsu CJ, Peng R, Jiang N, Xu XH, Ma YG, Liu D, Lu HD. Osteoporos. Int. 2022;33(10):2137-53.
- Adami G, Fassio A, Gatti D, Viapiana O, Benini C, Danila MI, Saag KG, Rossini M. Ther. Adv. Musculoskelet. Dis. 2022; 14:1759720X221083541.
- Rojas VP. Masa ósea reducida e hipovitaminosis D en mujeres posmenopáusicas: estudio exploratorio en Villavicencio, Colombia. 2012-2013. Arch. Med. (En línea).2015.
- Sarkar M, Bhardwaj R, Madabhavi I, Khatana J. Clin. Med. Insights: Circ. Respir. Pulm. Med. 2015 ;9: CCRPM-S22803.
- Ji MX, Yu Q. Chronic Dis Transl Med 2015;1(01):9-13.
- Stein E, Shane E. Endocrinol. Metab. Clin. N. Am.2003;32(1):115-34.
- Briot K, Roux C. RMD Open. 2015;1(1).
- Guañabens N, Gifre L, Peris P. Curr. Osteoporos. Rep. 2014;12(1):90-7.
- Hildebrandt S, Baschant U, Thiele S, Tuckermann J, Hofbauer LC, Rauner M. Sci. Rep. 2018;8(1):8711.
- Abdelfattah MA, Mohamed AS, Ibrahim SA, Fahmy SR.Sci. Rep. 2023;13(1):2090.
- Xi JC, Zang HY, Guo LX, Xue HB, Liu XD, Bai YB, Ma YZ. J. Recept. Signal Transduct. 2015;35(6):640-5.
- Pan JM, Wu LG, Cai JW, Wu LT, Liang M. J. Recept. Signal Transduct. 2019;39(1):80-6.
- Kimball JS, Johnson JP, Carlson DA. J Bone Joint Surg Am. 2021;103(15):1451-61.
- Barreca D, Laganà G, Bruno G, Magazù S, Bellocco E. Biochimie. 2013;95(11):2042-9.
- Silverman S, Christiansen C. Osteoporos. Int. 2012;23(3):797-809.
- Pinkerton JV, Thomas S, Dalkin AC. Clin. Obstet. Gynecol.
- Modi A, Sajjan S, Gandhi S. Int. J. Women's Health. 2014:759-69.
- Kennel KA, Drake MT. Mayo Clin Proc 2009 (Vol. 84, No. 7, pp. 632-638). Elsevier.
- Khosla S, Burr D, Cauley J, Dempster DW, Ebeling PR, Felsenberg D, Gagel RF, Gilsanz V, Guise T, Koka S, McCauley LK J. Bone Miner. Res. 2007;22(10):1479-91.
- McLachlan JM, Marx GM, Bridgman M. Med. J. Aust. 2013;199(4):242-3.
- Laaraj S, Ouahidi I, Aarab L. Egypt J Immunol. 2023;30(1):87-95.
- Gao L, Li H, Li B, Shao H, Yu X, Miao Z, Zhang L, Zhu L, Sheng H. J. Ethnopharmacol. 2022; 294:115387.
- Zhu Q, Zhang P, Liu D, Tang L, Yu J, Zhang C, Jiang G. Front. Nutr.. 2024; 11:1442535.
- Tubachi SS, Rasal VP, Ugare SR, Khatib NA, Ojha PS, Patil VS. Adv. Tradit. Med. 2023 ;23(2):575-88.
- Gudasi S, Gharge S, Koli R, Kagawad P. Chem. Biodivers. 2024;21(3):e202302072.
- Desaipatti R, Kudatarkar N, Gudasi S. J. Appl. Pharm. Sci. 2025;15(3):248-59.
- Gudasi S, Patil MB, Gharge S, Khatib NA. Netw. Model. Anal. Health Inform. Bioinform. 2025;14(1):131.
- Gudasi S, Patil MB, Gharge S, Ranade SD, Fanai HL, Chand J, Ahmad SF, Attia SM, Emran TB. Sci. Rep. 2025;15(1):32747.
- Kambalyal AM, Bhandurge P, Gawas N, Koli R, Gudasi S, Shetty P, Maste M, Gaikwad K. Nat. Prod. Res. 2024:1-9.
- Gharge S, Balikai CV, Gudasi S. Asp. Mol. Med. 2025; 5:100079.
- Gudasi S, Patil MB, Gharge S, Koli R, Khatib NA. ChemistrySelect. 2025 ;10(38): e01920. Gudasi S, Kumar D, Tewari S, Kavalapure RS, Ranade SD. Sci. Rep. 2025.
- Pote S, Salve P, Gudasi S, Gurav S. J. Herb. Med. 2025; 52:101038.
- Gudasi S, Gharge S, Kumar D, Tewari S, Ranade SD. J. Mol. Struct. 2026 :145555.
- Gudasi S, Gharge S, Koli R, Patil K. Futur. J. Pharm. Sci. 2023;9(1):25.
- Baliyan S, Mukherjee R, Priyadarshini A, Vibhuti A, Gupta A, Pandey RP, Chang CM. Molecules. 2022;27(4):1326.
- Sreejayan XX, Rao MN. J. Pharm. Pharmacol. 1997;49(1):105-7.
- Sulastri E, Zubair MS, Anas NI, Abidin S, Hardani R, Yulianti R. Pharmacogn. J. 2018;23(6).
- Hsu CH, Hsu CL, Langley A, Wojcik C, Iraganje E, Grygiel-Górniak B. Drugs Ther. Perspect. 2024;40(8):315-29.
- Frenkel B, White W, Tuckermann J. 2015:179-215.

- Wu Z, Li W, Jiang K, Lin Z, Qian C, Wu M, Xia Y, Li N, Zhang H, Xiao H, Bai J. MedComm. 2024;5(8): e657.
- Li B, Wang P, Jiao J, Wei H, Xu W, Zhou P. Front. Immunol. 2022; 13:824117.
- Gu J, Qin W, Feng P, Li C, Qi B, Zhang B, Dong Y. Zuo Gui Wan.
- Jiang T, Hu G, Yang R, Guan Z. J. Med. Food. 2024;27(9):824-33.
- Menteş M, Karakuzulu BB, Uçar GB, Yandım C. Comput. Biol. Chem. 2022; 99:107726.
- Zhu J, Ke K, Xu L, Jin J. J. Mol. Model. 2019;25(8):242.
- Zhang N, Ren Y, Xu Y. Front. Nutr. 2025; 12:1627949.